A Semi-Analytical Study of Stick-Slip Oscillations in Drilling Systems

B. Besselink
e-mail: b.besselink@tue.nl

N. van de Wouw
e-mail: n.v.d.wouw@tue.nl

H. Nijmeijer
e-mail: h.nijmeijer@tue.nl

Department of Mechanical Engineering,
Eindhoven University of Technology,
P.O. Box 513,
5600 MB Eindhoven,
The Netherlands

Rotary drilling systems are known to exhibit torsional stick-slip vibrations, which decrease drilling efficiency and accelerate the wear of drag bits. The mechanisms leading to these torsional vibrations are analyzed using a model that includes both axial and torsional drill string dynamics, which are coupled via a rate-independent bit-rock interaction law. Earlier work following this approach featured a model that lacked two essential aspects, namely, the axial flexibility of the drill string and dissipation due to friction along the bottom hole assembly. In the current paper, axial stiffness and damping are included, and a more realistic model is obtained. In the dynamic analysis of the drill string model, the separation in time scales between the fast axial dynamics and slow torsional dynamics is exploited. Therefore, the fast axial dynamics, which exhibits a stick-slip limit cycle, is analyzed individually. In the dynamic analysis of a drill string model without axial stiffness and damping, an analytical approach can be taken to obtain an approximation of this limit cycle. Due to the additional complexity of the model caused by the inclusion of axial stiffness and damping, this approach cannot be pursued in this work. Therefore, a semi-analytical approach is developed to calculate the exact axial limit cycle. In this approach, parametrized parts of the axial limit cycle are computed analytically. In order to connect these parts, numerical optimization is used to find the unknown parameters. This semi-analytical approach allows for a fast and accurate computation of the axial limit cycles, leading to insight in the phenomena leading to torsional vibrations. The effect of the (fast) axial limit cycle on the (relatively slow) torsional dynamics is driven by the bit-rock interaction and can thus be obtained by averaging the cutting and wearflat forces acting on the drill bit over one axial limit cycle. Using these results, it is shown that the cutting forces generate an apparent velocity-weakening effect in the torsional dynamics, whereas the wearflat forces yield a velocity-strengthening effect. For a realistic bit geometry, the velocity-weakening effect is dominant, leading to the onset of torsional vibrations. [DOI: 10.1115/1.4002386]

1 Introduction

Rotary drilling systems using drag bits, as used for the exploration and production of oil and gas, are known to experience different types of oscillations, which can be categorized as lateral, axial, and torsional vibrations. These vibrations might lead to whirling, bit bouncing, and (torsional) stick-slip, respectively [1–6]. In the current work, the focus is on the axial and torsional vibrations. Torsional stick-slip is characterized by phases where the rotation of the bit completely stops (stick) and phases where the bit reaches rotational speeds of up to two times the nominal rotational speed (slip). These stick-slip oscillations decrease the drilling efficiency, accelerate the wear of drag bits, and may even lead to drill string failure because of fatigue.

In the analysis of the torsional vibrations, most studies rely on one or two degree-of-freedom models that account for the torsional dynamics only. Usually, the resisting torque at the bit-rock interface is modeled by trivializing it as a frictional contact. Common friction models include a (locally) velocity-weakening effect [7–10] and Coulomb friction [11]. These friction models are based on experimental results [7,12] that show a decrease in the torque-on-bit for increasing rotational speed. In these models, the rate effect is thus seen as an intrinsic property of the processes taking place at the bit-rock interface. However, it has to be noted that these experimental results are obtained by averaging the torque-on-bit over multiple revolutions and may not hold at a faster, more relevant time scale. Moreover, bit-rock interaction experiments using single cutters have not revealed any intrinsic velocity-weakening effect [13]. Instead, the cutting forces remain constant for a large range of cutting velocities. Therefore, the observed velocity-weakening effect on full drill bits is likely to be the result of complex drill string dynamics, rather than an intrinsic property of the bit-rock interaction.

This insight has led to a different approach for modeling the dynamics of drilling systems. Based on the rate-independent bit-rock interaction model presented in Refs. [14,15], a drill string model is presented in Refs. [16,17]. In this approach, the axial and torsional dynamics are coupled via the bit-rock interaction law, which generates a regenerative effect [18,19] due to the cutting forces, as well as contact forces. Furthermore, the axial and torsional dynamics are described by lumped-parameter models as opposed to more complex models such as a continuum approach [20] or finite-element formulations [21]. This approach is motivated by results from Ref. [22], where it is shown that the lumped-parameter approach gives a good qualitative description of the phenomena as observed in more complex finite-element models. Furthermore, the lumped-parameter approach allows for an in-depth analysis, providing insight in the mechanisms leading to vibrations, as in Ref. [23]. Here, it is shown that the axial and torsional dynamics can be studied individually because of the difference in time scales. An analysis of the fast axial dynamics shows the existence of an axial stick-slip limit cycle, whose properties are dependent on the rotational speed. This serves as the driving force behind an apparent velocity-weakening effect in the torsional dynamics, leading to torsional vibrations and stick-slip. Hence, the axial dynamics is responsible for the onset of torsional vibrations.

Contributed by the Design Engineering Division of ASME for publication in the Journal of Computational and Nonlinear Dynamics. Manuscript received October 14, 2009; final manuscript received June 23, 2010; published online October 22, 2010. Assoc. Editor: Alain Berlioz.

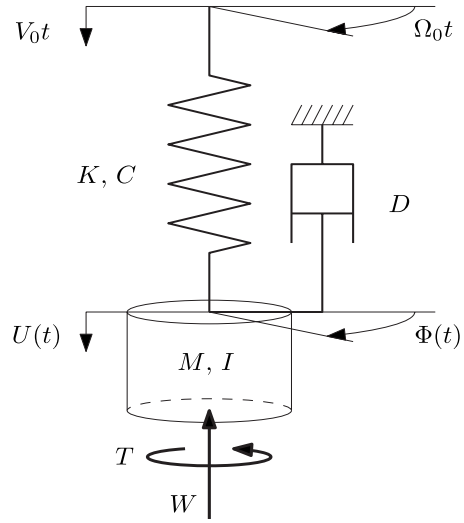

Fig. 1 Schematic model of a drill string

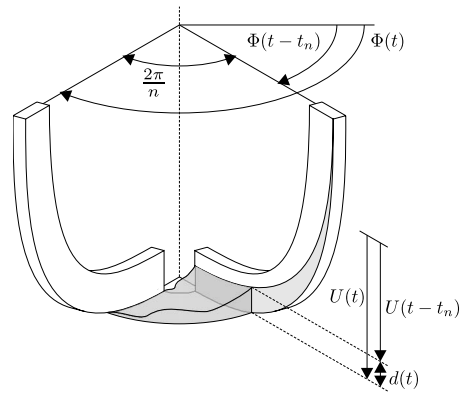

Fig. 2 Bottom hole profile between two successive blades (after Ref. [16])

In the approach in Refs. [16,17,23], the drill string is modeled as a single lumped inertia in the axial direction. It is thus assumed that the weight-on-bit is constant, which can be achieved by controlling the hook load. However, this implies that the axial movement of the drill string at the surface has to match the axial displacement of the drill bit in order not to compress or relax the drill string. Since the bit experiences high-frequency axial vibrations, this is unrealistic.

Therefore, in the current work, the finite axial stiffness of the drill string is taken into account, where it is assumed that the axial position of the drill string is prescribed at the surface. Further, axial viscous damping is included to model the effect of dissipation due to friction along the bottom hole assembly (BHA). Both effects are thus relevant in practice such that the model extensions lead to a more realistic model. Here, the main question is whether this updated model still predicts the onset of torsional vibrations and stick-slip, as observed in experiments on drilling rigs and captured by the original model in Ref. [23]. Because of the additional model complexity caused by the axial stiffness and damping, the approach as presented in Ref. [23], where an *approximation* of the axial stick-slip limit cycle was obtained analytically, cannot be pursued. Therefore, a semi-analytical approach is developed to obtain the *exact* axial limit cycle. In this approach, parametrized analytical solutions are derived for different parts of the axial limit cycle, whereas numerical optimization is used to obtain the unknown parameters leading to an exact characterization of the full limit cycle. Next, it is shown that the axial dynamics generate an apparent velocity-weakening effect in the torsional direction, forming the onset of torsional vibrations.

This paper is organized as follows. The drill string model will be discussed in Sec. 2. Next, the axial limit cycle will be analyzed using a semi-analytical approach in Sec. 3. The obtained results on the axial dynamics will be used to analyze the torsional dynamics in Sec. 4. Finally, conclusions will be presented in Sec. 5.

2 Modeling of Drilling Dynamics

The model of a drill string setup is depicted in Fig. 1. The BHA with axial and angular positions U and Φ, respectively, is modeled as a discrete mass M with inertia I. The drill string is modeled as a spring with torsional stiffness C and axial stiffness K. At the top, both the axial and angular displacements are prescribed. This represents the rotary table, which is assumed to exhibit the constant rotational and vertical speeds, Ω_0 and V_0, respectively. The viscous friction parameter D characterizes viscous friction along the BHA, leading to the equations of motion for the BHA as

$$M\frac{d^2U}{dt^2} + D\frac{dU}{dt} + K(U - V_0t) = -W^c - W^f \tag{1}$$

$$I\frac{d^2\Phi}{dt^2} + C(\Phi - \Omega_0t) = -T^c - T^f \tag{2}$$

Here, W and T respectively denote the force and torque on the drill bit as a result of the bit-rock interaction. This consists of a cutting and friction component, denoted by superscripts c and f, respectively. The cutting process takes place on the cutting face of the blades on the drill bit and describes the removal of the rock, whereas the friction component is caused by the contact between the underside of the blades (called the wearflat) and the well bottom. Following Ref. [14], these processes are modeled by

$$W^c = na\zeta\varepsilon d, \quad W^f = nal\bar{\sigma}\frac{1+\mathrm{sgn}(dU/dt)}{2} \tag{3}$$

$$T^c = \frac{1}{2}na^2\varepsilon d, \quad T^f = \frac{1}{2}na^2\xi\mu l\bar{\sigma}\frac{1+\mathrm{sgn}(dU/dt)}{2} \tag{4}$$

with n the number of blades on the drill bit with radius a. The cutting process is characterized by the intrinsic specific energy ε, which gives the required energy to destroy a unit volume of rock, and the orientation of the cutting face, represented by ζ. The frictional process takes place on the bit-rock interface with length l at the underside of the blades, known as the wearflat. The bit-rock contact at the wearflats is described by the contact stress, which is constant (and equal to $\bar{\sigma}$) when the bit moves downward into the rock. The contact force is thus independent of the magnitude of the axial velocity. This is confirmed by experimental results presented in Ref. [15], which show that the forces due to the bit-rock interaction are indeed rate independent. Further, the geometry of the bit-rock contact indicates that the wearflat is no longer in contact with the rock when the bit moves upward. This is modeled using the sign function in W^f. A frictional process at the wearflat relates this contact force W^f to the friction torque T^f via the friction coefficient μ and the parameter γ, which characterizes the spatial distribution of the wearflats. Finally, the cutting forces are proportional to the depth-of-cut d, which is in general not constant. Specifically, the depth-of-cut depends on the axial position of the cutter with respect to the rock surface, as generated by the previous blade some time t_n ago. This is schematically depicted in Fig. 2. Hence, the depth-of-cut, describing the height of material in front of a single blade, can be written as

$$d(t) = U(t) - U(t - t_n(t)) \tag{5}$$

The delay t_n itself is time dependent and denotes the time interval in which the bit rotates $2\pi/n$ rad, which is the angle between two successive blades:

$$\int_{t-t_n(t)}^{t} \frac{d\Phi(s)}{ds} ds = \Phi(t) - \Phi(t - t_n(t)) = \frac{2\pi}{n} \tag{6}$$

In the calculation of the depth-of-cut and the delay, it is assumed that the drill bit moves down a perfectly vertical well. Lateral motions of the drill bit (i.e., bit whirl) are not considered.

The equations of motion are scaled to reduce the number of parameters. Thereto, the characteristic time scale $t_* = \sqrt{I/C}$ and length $L_* = 2C/\varepsilon a^2$ are introduced. Here, $2\pi t_*$ is the period time related to the torsional resonance frequency. The characteristic length L_* represents the depth-of-cut (for one revolution of the drill bit) for a perfectly sharp cutter inducing a one radian twist in the drill string. Typically, $t_* \sim 1$ s and $L_* \sim 1$ mm. These characteristic parameters are used in coordinate transformation,

$$u(\tau) = \frac{U - U_0}{L_*}, \quad \varphi(\tau) = \Phi - \Phi_0 \tag{7}$$

where u and φ are functions of the dimensionless time $\tau = t/t_*$ and represent the (scaled) relative axial and angular velocities, respectively. Next, $U_0(t)$ and $\Phi_0(t)$ are the equilibrium solutions of Eqs. (1) and (2), respectively. These equilibria are the trivial solutions in the absence of vibrations and correspond to a constant axial and torsional velocities since the drill bit has to follow the imposed velocities V_0 and Ω_0. The coordinate transformation leads to

$$\ddot{u}(\tau) + \gamma\dot{u}(\tau) + \eta^2 u(\tau) = n\psi[-v_0(\tau_n - \tau_{n0}) - u(\tau) + u(\tau - \tau_n) + \lambda g(\dot{u}(\tau))] \tag{8}$$

$$\ddot{\varphi}(\tau) + \varphi(\tau) = n[-v_0(\tau_n - \tau_{n0}) - u(\tau) + u(\tau - \tau_n) + \beta\lambda g(\dot{u}(\tau))] \tag{9}$$

$$\varphi(\tau) - \varphi(\tau - \tau_n) + \omega_0\tau_n = 2\pi/n \tag{10}$$

where the dot denotes differentiation with respect to the dimensionless time τ. It is noted that the equilibrium $u = \varphi = 0$ corresponds to constant drilling, with positive and constant axial and torsional velocities. The parameters γ and η are the scaled axial damping and viscous friction, whereas ψ characterizes the drill string design:

$$\gamma = \frac{D}{M}\sqrt{\frac{I}{C}}, \quad \eta = \sqrt{\frac{KI}{MC}}, \quad \psi = \frac{\zeta\varepsilon a I}{MC} \tag{11}$$

The influence of wearflat friction is given by λ, which is a measure of the bluntness of the bit and therefore equals zero for perfectly sharp cutters. The parameter β groups the parameters ζ, μ, and ξ and characterizes the drill bit design:

$$\lambda = \frac{a^2 l\bar{\sigma}}{2\zeta C}, \quad \beta = \zeta\mu\xi \tag{12}$$

Because of scaling, all parameters are of $\mathcal{O}(1)$. The only exception is ψ, which, for a large class of drilling systems, is typically of $\mathcal{O}(10^2 - 10^3)$. This fact will be exploited later. The nonlinear function $g(\dot{u}(\tau))$ describes whether the wearflat is in contact with the rock ($g=0$) or not ($g=1$). Following Filippov's solution concept, the discontinuity at $\dot{u} = -v_0$ ($dU/dt = 0$) is replaced by a convex set-valued map:

$$g(\dot{u}(\tau)) \in \frac{1 - \mathrm{Sgn}(\dot{u}(\tau) + v_0)}{2} = \begin{cases} 0, & \dot{u} > -v_0 \\ [0,1], & \dot{u} = -v_0 \\ 1, & \dot{u} < -v_0 \end{cases} \tag{13}$$

where $\mathrm{Sgn}(\cdot)$ is the set-valued sign function. Hence, the model in Eqs. (8)–(10) and the set-valued map in Eq. (13) constitute a delay-differential inclusion, of which the oscillatory behavior will be analyzed.

It has to be noted that the model in Eqs. (8)–(10) is only valid when the bit rotates in the positive direction ($\dot{\varphi} > -\omega_0$), and the blades either remove the material ($d > 0$) or slide on the bottom of the borehole ($d = 0$). This results in two phases where the model in the current form loses validity, namely, bit bouncing and torsional stick.

Bit bouncing is characterized by a negative depth-of-cut d, indicating that the bit is no longer in contact with the rock. It can be caused by large axial vibrations and causes damage to the drill bit. Bit bouncing should therefore be avoided at all times and is not analyzed in this work.

Even though torsional stick is not included in the formulation in Eqs. (8)–(10), this model can be used to predict the *onset* of torsional vibrations. These mechanisms leading to torsional vibrations (and stick-slip) are the main interest of this study.

Nonetheless, torsional stick can be included in the model as follows. Thereto, it is assumed that the frictional torque on the wearflat is sufficient to prevent the bit from rotating backward, which is a realistic assumption in practice. Therefore, when the rotational speed $d\Phi/dt$ becomes zero, the bit sticks to the rock ($\dot{\varphi}(\tau) = -\omega_0$) and no longer removes material. It is assumed that the rock underneath the bit cannot be indented, implying that the bit also sticks in the axial direction ($\dot{u}(\tau) = -v_0$). Since the axial dynamics is modeled as a single inertia, this implies the total absence of axial drill string vibrations during a torsional stick phase. Physically, torsional stick is caused when the torque applied to the bit is insufficient to overcome the cutting and friction torque needed to drill. However, because of the continuous rotation of the rotary table at the surface, the drill string is twisted, increasing the torque applied to the drill bit. The bit starts moving again when this force is sufficient to overcome the reacting torque and generates a positive angular acceleration (for all $g^* \in [0,1]$):

$$n[-v_0(\tau_n - \tau_{n0}) - u(\tau) + u(\tau - \tau_n) + \beta\lambda g^*] - \varphi(\tau) > 0. \tag{14}$$

Contrary to models commonly used for the the analysis of torsional vibrations, the model used in the current work is based on a rate-independent bit-rock interaction law, which couples the axial and torsional dynamics. In this section, the model in Refs. [16,17,23] is extended by incorporating the important effects of the finite axial stiffness of the drill string as well as the axial friction along the BHA. In Secs. 3 and 4, it will be shown that axial stick-slip vibrations lead to an apparent velocity-weakening effect of the torque-on-bit, which forms the onset of torsional vibrations and stick-slip. Hereto, in Sec. 3, a semi-analytical analysis approach providing an *exact* characterization of the axial limit cycle is developed for the extended model, as opposed to the *approximate* analysis in Ref. [23], for a model without axial drill string flexibility and axial dissipation.

3 Axial Dynamics

For a broad class of drilling systems, the magnitude of the parameter ψ, which is of $\mathcal{O}(10^2 - 10^3)$, implies that the axial dynamics in Eq. (8) is fast when compared with the torsional dynamics in Eq. (9) [23]. This implies that, for this class of systems, the axial dynamics can be analyzed individually, where the slowly varying rotational speed can be considered constant. To emphasize the fast time scale of the axial dynamics, the stretched time $\bar{\tau} = \tau\sqrt{n\psi}$ is introduced.

In steady-state drilling, the average axial velocity (over multiple revolutions) of the drill bit should equal the imposed axial velocity at the surface in order for the drill string length to be constant on average. Any periodic motions in the axial velocity

are therefore not periodic in the axial position, as required to find true periodic orbits. Therefore, the coordinate transformation,

$$z_1(\bar{\tau}) = \frac{-\bar{v}_0(\bar{\tau}_n - \bar{\tau}_{n0}) - u(\bar{\tau}) + u(\bar{\tau} - \bar{\tau}_n) - \bar{\eta}^2 u(\bar{\tau}) - \bar{\gamma} u'(\bar{\tau})}{\bar{v}_0} \tag{15}$$

$$z_2(\bar{\tau}) = \frac{u'(\bar{\tau})}{\bar{v}_0} \tag{16}$$

is introduced. Physically, z_1 is a scaled version of the deviation from the nominal forces acting on the drill bit, except the wearflat force. The coordinate z_2 is a scaled version of the relative axial velocity in stretched time, where $'$ denotes differentiation with respect to the stretched time $\bar{\tau}$. The application of the coordinate transformation to Eq. (8) yields the dynamics

$$z_1'(\bar{\tau}) = -(1 + \bar{\eta}^2) z_2(\bar{\tau}) + z_2(\bar{\tau} - \bar{\tau}_n) - \bar{\gamma} z_1(\bar{\tau}) - \bar{\gamma} \frac{\lambda}{\bar{v}_0} \hat{g}(z_2(\bar{\tau})) \tag{17}$$

$$z_2'(\bar{\tau}) = z_1(\bar{\tau}) + \frac{\lambda}{\bar{v}_0} \hat{g}(z_2(\bar{\tau})) \tag{18}$$

with

$$\hat{g}(z_2(\bar{\tau})) \in \frac{1 - \mathrm{Sgn}(z_2(\bar{\tau}) + 1)}{2} \tag{19}$$

and

$$\bar{\gamma} = \frac{\gamma}{\sqrt{n\psi}}, \quad \bar{\eta} = \frac{\eta}{\sqrt{n\psi}}, \quad \bar{v}_0 = \frac{v_0}{\sqrt{n\psi}} \tag{20}$$

where $\bar{\gamma}$ and $\bar{\eta}$ are of $\mathcal{O}(0.1)$.

From Eqs. (17) and (18), it can be seen that the equilibrium point is at $z_1 = z_2 = 0$, corresponding to a constant drilling velocity. Hence, periodic oscillations will appear as periodic orbits in these new coordinates.

A major advantage of the coordinate transform is that the new set of equations requires the delayed axial velocity $z_2(\bar{\tau} - \bar{\tau}_n) = u'(\bar{\tau} - \bar{\tau}_n)/\bar{v}_0$ instead of the delayed position $u(\bar{\tau} - \bar{\tau}_n)$. In the stick phase, the axial velocity is explicitly known ($dU/dt = 0 \Leftrightarrow z_2 = -1$), which is beneficial for the analysis of the axial limit cycle in Sec. 3.2. It allows for the calculation of analytical solutions for parts of the limit cycle. This is a highly efficient way of calculating the axial limit cycles, compared with the usage of periodic solvers such as the shooting method or numerical integration, for example.

3.1 Axial Stability Analysis. By construction of the coordinate transformation, the equilibrium solution of Eqs. (17)–(19) equals $z_1 = z_2 = 0$. Physically, this corresponds to a constant drilling velocity. Therefore, around the equilibrium point, the full contact stress is active. Stated differently, the nonlinearity $\hat{g}(z_2(\bar{\tau}))$ equals 0, as can also be concluded from Eq. (19). Therefore, the local stability of the equilibrium $(z_1, z_2) = (0, 0)$ can be investigated by considering the roots of the characteristic equation,

$$P(s) = s^2 + \bar{\gamma} s + \bar{\eta}^2 + 1 - e^{-s\bar{\tau}_n} = 0 \tag{21}$$

Stability properties are determined in two steps. First, the roots of Eq. (21) are calculated for $\bar{\tau}_n = 0$. Second, Eq. (21) is evaluated at the imaginary axis ($s = i\omega$) in order to track any roots crossing the imaginary axis for increasing delay $\bar{\tau}_n$.

The results of a stability analysis for varying dimensionless stiffness parameter $\bar{\eta}$ and delay $\bar{\tau}_n$, which is inversely proportional to the rotational speed of the BHA, can be found in Fig. 3. From the top graph, where no axial damping is present, it is clear that, for small $\bar{\eta}$, the range in the delay for which the equilibrium point is locally asymptotically stable decreases with increasing stiffness. For higher stiffness, multiple stability regions emerge, caused by the complex interaction between the dynamics and the delay. The bottom graph (for $\bar{\gamma} = 0.5$) shows that the parameter region for which the dynamics is locally asymptotically stable increases for increasing delay, as the axial damping is increased. However, for realistic values of the stiffness, damping (both of $\mathcal{O}(0.1)$), and delay (of $\mathcal{O}(10-10^2)$), the axial equilibrium point is unstable.

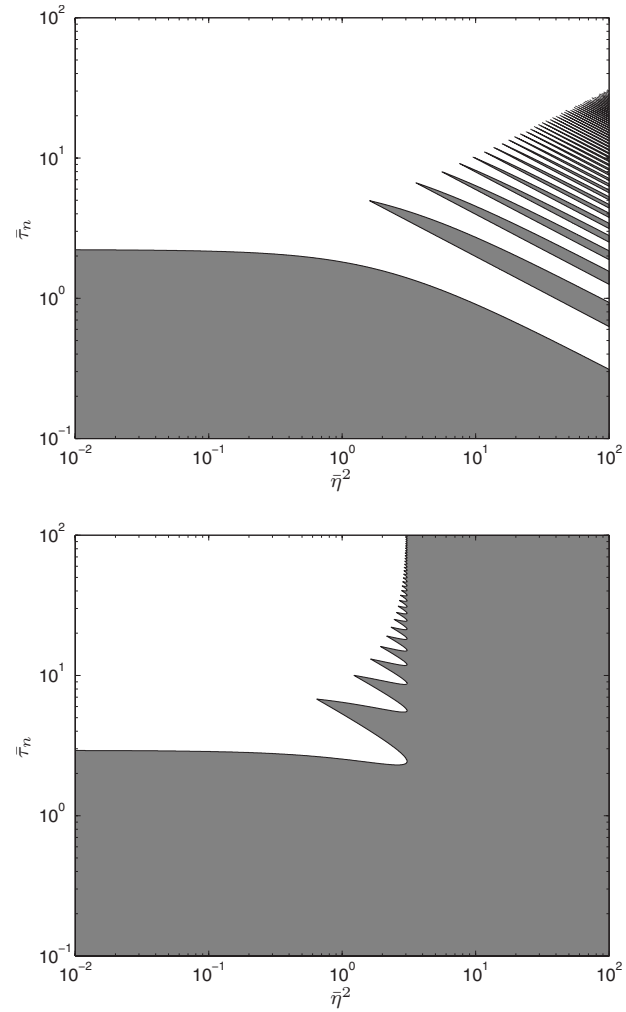

Fig. 3 Stability diagram in $(\bar{\eta}^2, \bar{\tau}_n)$-space for $\bar{\gamma}=0$ (top) and $\bar{\gamma}=0.5$ (bottom). The stable region is depicted in gray, and the unstable region is depicted in white.

For these parameter values, small perturbations around the equilibrium point grow. Numerical simulations show that these perturbations result in an axial limit cycle, which is analyzed in more detail in the next section.

3.2 Axial Limit Cycle Analysis. A typical example of the axial limit cycle in (z_1, z_2) coordinates is shown in the top graph of Fig. 4, which gives the time series of z_1 and z_2 as well as the delayed coordinate $\tilde{z}_2(\bar{\tau}) = z_2(\bar{\tau} - \bar{\tau}_n)$ and the nonlinearity $\hat{g}$. The bottom graph shows the corresponding absolute position U and velocity dU/dt. In these absolute coordinates, no limit cycle can be observed because of the drift in the axial position, caused by the nominal downward velocity. The limit cycle consists of two distinct phases that can be recognized in both figures: the *slip phase* and the *stick phase*.

The slip phase (for $\bar{\tau} \in [0, \bar{\tau}_a + \bar{\tau}_b]$) has a length of $\bar{T}_{\mathrm{slip}} = \bar{\tau}_a + \bar{\tau}_b$ and is characterized by a positive axial velocity $dU/dt > 0$ (i.e., $z_2 > -1$). Here, the bit penetrates the rock and moves downward. In Fig. 4, this phase is highlighted by a black bar. Since the bit moves downward, the full contact stress is mobilized and $\hat{g} = 0$.

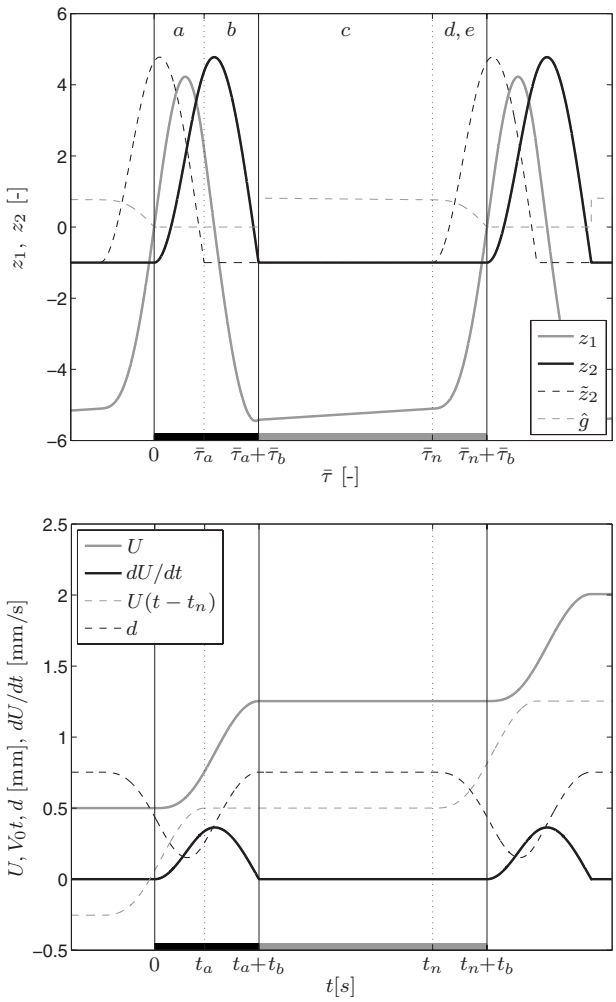

Fig. 4 Example of an axial limit cycle in (z_1, z_2) coordinates (top) and $(U, dU/dt)$ coordinates (bottom)

Evaluating Eq. (18) for $\hat{g}=0$ gives $z_2'=z_1$, such that z_1 represents the scaled acceleration of the bit. A stick phase is entered when the axial velocity dU/dt drops to zero, where the wearflat forces can accommodate variations in the other forces acting on the bit.

The stick phase (for $\bar{\tau}\in[\bar{\tau}_a+\bar{\tau}_b, \bar{\tau}_n+\bar{\tau}_b]$) has a length of $\bar{T}_{\text{stick}}=\bar{\tau}_n-\bar{\tau}_a$ and is characterized by a zero axial velocity $dU/dt=0$ (i.e., $z_2=-1$). This phase is highlighted by a gray bar in Fig. 4. Because of the positive rotational speed, the bit still removes the rock, as can be concluded from the positive depth-of-cut d. The stick phase is caused by the discontinuity in the contact forces at zero axial velocity, which can entirely compensate the other forces acting on the bit. As the depth-of-cut decreases, caused by the change in the rock profile left by the previous blade, the wearflat forces can no longer accommodate for the decreasing cutting forces and the bit enters a new slip phase.

During a large part of the stick phase, the depth-of-cut is constant, as can be seen in Fig. 4. This is caused by the overlap in the angular position of the current and previous stick phases. At the angular position the bit started moving axially during the previous rotation, the depth-of-cut decreases. In order to maintain the stick phase, the wearflat forces will increase until the maximum force is reached ($\hat{g}=0$). Then, the bit will start to move axially again, entering another slip phase. Since the wearflat forces can accommodate for some decrease in d, the period of the limit cycle is slightly higher than the delay.

In Secs. 3.3 and 3.4, the slip and stick phase will be analyzed, respectively.

3.3 Slip Phase. In the slip phase, the full contact stress is active and the nonlinearity $\hat{g}$ equals zero. Substituting this in Eqs. (17) and (18) leads to the following linear delay-differential equations:

$$z_1'(\bar{\tau}) = -(1+\bar{\eta}^2)z_2(\bar{\tau}) + z_2(\bar{\tau}-\bar{\tau}_n) - \bar{\gamma}z_1(\bar{\tau}) \tag{22}$$

$$z_2'(\bar{\tau}) = z_1(\bar{\tau}) \tag{23}$$

As can be seen in Fig. 4, the slip phase is split in parts a and b, which are chosen such that the delayed scaled velocity $\tilde{z}_2(\bar{\tau})=z_2(\bar{\tau}-\bar{\tau}_n)$ is constant and equals -1 in phase b (for $\bar{\tau}\in[\bar{\tau}_a, \bar{\tau}_a+\bar{\tau}_b]$). Furthermore, by the choice of the parts a of b, the delayed velocity $\tilde{z}_2(\bar{\tau})=z_2(\bar{\tau}-\bar{\tau}_n)$ in phase a (for $\bar{\tau}\in[0, \bar{\tau}_a]$) equals the nondelayed $z_2(\bar{\tau})$ in phase b. It is therefore convenient to calculate the solution in phase b first and consider the dynamics in the reversed time $\bar{\tau}_r=-\bar{\tau}$:

$$\dot{\boldsymbol{z}}(\bar{\tau}_r) = \boldsymbol{A}\boldsymbol{z}(\bar{\tau}_r) + \boldsymbol{B}\tilde{z}_2 \tag{24}$$

Here, ` denotes differentiation with respect to the reversed time $\bar{\tau}_r$. The term $z_2(\bar{\tau}_r+\bar{\tau}_n)$ is known and can therefore be considered as an input $\tilde{z}_2(\bar{\tau}_r)=z_2(\bar{\tau}_r+\bar{\tau}_n)$ to a set of linear equations, which yields the standard linear state-space form with state $\boldsymbol{z}=[z_1, z_2]^{\mathrm{T}}$ and system matrices,

$$\boldsymbol{A} = \begin{bmatrix} \bar{\gamma} & 1+\bar{\eta}^2 \\ -1 & 0 \end{bmatrix}, \quad \boldsymbol{B} = \begin{bmatrix} -1 \\ 0 \end{bmatrix} \tag{25}$$

3.3.1 Phase b. The total solution in phase b can now be obtained as the solution to Eq. (24) for the delayed velocity $\tilde{z}_2=-1$ and the initial condition $\boldsymbol{z}^b(0)=[z_{1,\min}, -1]^{\mathrm{T}}$. Here, $z_{1,\min}=z_1(\bar{\tau}_a+\bar{\tau}_b)$ is an unknown, which will be determined later. It represents the minimum value of $z_1(\bar{\tau})$ in the stick phase, which is not necessarily the overall minimum value. The solution in phase b is given as a function of the local (reversed) time $\bar{\tau}_r^b=\bar{T}_{\text{slip}}-\bar{\tau}$ and reads

$$\boldsymbol{z}^b(\bar{\tau}_r^b) = e^{\boldsymbol{A}\bar{\tau}_r^b}\boldsymbol{z}^b(0) - \int_0^{\bar{\tau}_r^b} e^{\boldsymbol{A}(\bar{\tau}_r^b-s)}\boldsymbol{B}ds \tag{26}$$

3.3.2 Phase a. As for phase b, the dynamics in phase a is described by Eq. (24), but with a different initial condition $\boldsymbol{z}_0$ and delayed velocity $\tilde{z}_2$, which serves as an input for the state-space model. The initial condition for the solution in phase a is given by the result of phase b as $\boldsymbol{z}^a(0)=\boldsymbol{z}^b(\bar{\tau}_b)$, whereas the delayed velocity $\tilde{z}_2^a$ equals the solution in phase b, as can be seen in Fig. 4. Then, the solution in phase a is given in the reversed local time as $\bar{\tau}_r^a=\bar{\tau}_a-\bar{\tau}$ as

$$\boldsymbol{z}^a(\bar{\tau}_r^a) = e^{\boldsymbol{A}\bar{\tau}_r^b}\boldsymbol{z}^a(0) + \int_0^{\bar{\tau}_r^a} e^{\boldsymbol{A}(\bar{\tau}_r^a-s)}\boldsymbol{B}z_2^b(s)ds \tag{27}$$

It has to be noted that the integrals in Eqs. (26) and (27) can easily be evaluated analytically. Next, since the solution z_2^b in phase b is used as an input for the linear dynamics in phase a, the solution for phase a can only be defined for $\bar{\tau}_r^a\in[0, \bar{\tau}_b]$. Stated differently, the length of phase a cannot exceed the length of phase b: $\bar{\tau}_a \le \bar{\tau}_b$. The validity of this condition will be checked in Sec. 3.5.

3.4 Stick Phase. The dynamics in Eqs. (17) and (18) in the stick phase is characterized by $z_2'=0$. Since the dynamics is considered in forward time, it can be described by

$$z_1'(\bar{\tau}) = (1+\bar{\eta}^2) + z_2(\bar{\tau}-\bar{\tau}_n) \tag{28}$$

$$0 = z_1(\bar{\tau}) + \frac{\lambda}{v_0}\hat{g}(-1) \tag{29}$$

The bit sticks axially because the wearflat forces can compensate entirely for the difference between cutting forces and forces exerted by the drill string. The value of the nonlinearity $\hat{g}$ is therefore prescribed by the value of $z_1(\bar{\tau})$ and can be obtained by evaluating Eq. (29). The stick phase is subdivided into phases c, d, and e, which will be discussed next.

3.4.1 Phase c. In phase c, both the current velocity z_2 and the delayed velocity $\tilde{z}_2$ equal -1. The solution in phase c can then be obtained by simply integrating Eq. (28) using the initial condition $z_1^c(0)=z_{1,\min}$, as introduced before. This leads to the solution as a function of the local time $\bar{\tau}^c=\bar{\tau}-\bar{T}_{\text{slip}}$:

$$z_1^c(\bar{\tau}^c) = z_{1,\min} + \bar{\eta}^2\bar{\tau}^c \tag{30}$$

$$z_2^c(\bar{\tau}^c) = -1 \tag{31}$$

The initial condition for the solution in phase d is given by the result for phase c:

$$z_1^d(0) = z_1(\bar{\tau}_n) = z_1^c(\bar{\tau}_n - \bar{T}_{\text{slip}}) = z_{1,\min} + \bar{\eta}^2(\bar{\tau}_n - \bar{T}_{\text{slip}}) \tag{32}$$

3.4.2 Phases d and e. As for phase c, the solution in phases d and e can be obtained by integrating Eq. (28). However, the delayed velocity $\tilde{z}_2$ is no longer constant. Since phase d starts at $\bar{\tau}=\bar{\tau}_n$, this delayed velocity equals the solution in the slip phase, as can also be concluded from Fig. 4. Using the local time $\bar{\tau}^d=\bar{\tau}-\bar{\tau}_n$, this can be expressed as

$$z_2^d(\bar{\tau}^d - \bar{\tau}_n) = z_2(\bar{\tau}^d) = z_2^a(\bar{\tau}_a - \bar{\tau}^d) \tag{33}$$

Here, it has to be recalled that phase a has a length of $\bar{\tau}_a$ and the solution z_2^a is given in reversed time, which explains the argument of z_2^a. Using this fact, the solution in phase d is given by

$$z_1^d(\bar{\tau}^d) = z_1^d(0) + (1+\bar{\eta}^2)\bar{\tau}^d + \int_0^{\bar{\tau}^d} z_2^a(\bar{\tau}_a - s)ds \tag{34}$$

$$z_2^d(\bar{\tau}^d) = -1 \tag{35}$$

Since the length of phase a is limited, the integral is only defined for $\bar{\tau}^d \in [0, \bar{\tau}_a]$. However, the combined length of phases d and e equals $\bar{\tau}_b$, which is larger than (or equal to) $\bar{\tau}_a$. Thus, in the final part with a length of $\bar{\tau}_b - \bar{\tau}_a$, the delayed velocity is given by the solution in phase b. Using the local time $\bar{\tau}^e=\bar{\tau}-\bar{\tau}_n-\bar{\tau}_a$, the solution in phase e is similar to that of phase d:

$$z_1^e(\bar{\tau}^e) = z_1^e(0) + (1+\bar{\eta}^2)\bar{\tau}^e + \int_0^{\bar{\tau}^e} z_2^b(\bar{\tau}_b - s)ds \tag{36}$$

$$z_2^e(\bar{\tau}^e) = -1 \tag{37}$$

Here, the initial condition reads $z_1^e(0)=z_1^d(\bar{\tau}_b)$.

3.5 Construction of the Total Solution. The axial limit cycle is calculated by dividing it in phases a to e, for which analytic expressions can be found. However, three unknown parameters remain. These parameters fully characterize the limit cycle and are the initial condition $z_{1,\min}$ and the lengths of phases a and b, being $\bar{\tau}_a$ and $\bar{\tau}_b$, respectively. To obtain these parameters, the limit cycle at $\bar{\tau}=0$ is considered first. At this point, the stick phase ends and a new slip phase is initiated, which gives the conditions

$$z_1(0) = z_1^a(\bar{\tau}_a) = 0 \tag{38}$$

$$z_2(0) = z_2^a(\bar{\tau}_a) = -1 \tag{39}$$

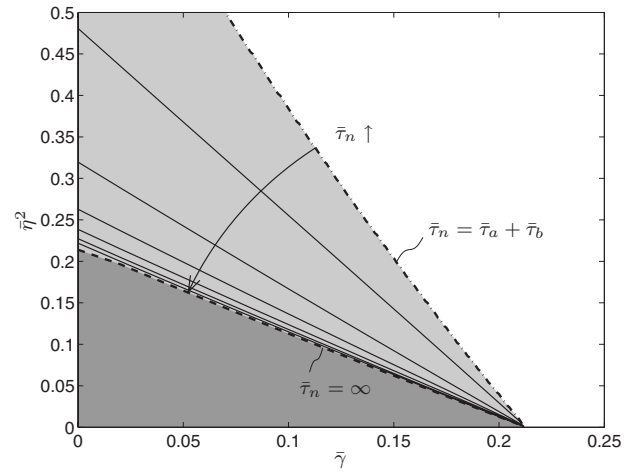

Fig. 5 Validity of the condition $\bar{\tau}_a \leq \bar{\tau}_b$ in $(\bar{\gamma}, \bar{\eta}^2)$-space. The dash-dotted line shows the line $\bar{\tau}_a = \bar{\tau}_b$ for the minimal delay. For increasing delay, the validity region decreases, as shown for $\bar{\tau}_n = \{5, 10, 20, 40, 80, 160\}$. Finally, the dashed line is a numerical approximate of the asymptote for $\bar{\tau}_n \to \infty$.

A third condition results from the properties of the limit cycle. In practice, both the relative velocity $\dot{u}$ and relative bit position u are periodic. For the bit position to be periodic, the average relative velocity over one limit cycle has to be zero. Obviously, this should also hold for the scaled velocity z_2, yielding

$$\int_0^{\bar{T}} z_2(s)ds = 0 \tag{40}$$

Here, $\bar{T}=\bar{T}_{\text{slip}}+\bar{T}_{\text{stick}}=\bar{\tau}_n+\bar{\tau}_b$ is the total period of the limit cycle.

Equations (38)–(40) are solved simultaneously using a numerical Nelder–Mead optimization scheme [24], as implemented in MATLAB, to obtain the values of $\bar{\tau}_a$, $\bar{\tau}_b$, and $z_{1,\min}$. However, it was shown that the analytical solution of the limit cycle is only valid for $\bar{\tau}_a \leq \bar{\tau}_b$ and $\bar{\tau}_a + \bar{\tau}_b \leq \bar{\tau}_n$. Here, the latter condition provides a lower bound for the delay, whereas the first condition can be shown to imply an upper bound for the delay. Typical values of the delay $\bar{\tau}_n$ are $\mathcal{O}(10-10^2)$, which in practice corresponds to drilling speeds of $\mathcal{O}(10-10^2)$ rpm. Since $\bar{\tau}_a+\bar{\tau}_b$ is of $\mathcal{O}(1)$, the lower bound is of little interest and focus is on the validity of the condition $\bar{\tau}_a \leq \bar{\tau}_b$, which is checked for a range in parameters in Fig. 5. In this figure, three regions can be distinguished. First, in the white region, no value of the delay $\bar{\tau}_n$ can be found satisfying both conditions. Next, in the gray regions there exist values $\bar{\tau}_n$ satisfying $\bar{\tau}_n \geq \bar{\tau}_a + \bar{\tau}_b$ and $\bar{\tau}_a \leq \bar{\tau}_b$, where it is recalled that the latter provides an upper bound on the delay. Therefore, for increasing delay $\bar{\tau}_n$, the validity region in parameter space decreases until the dark gray region remains, where the approximation is valid for all $\bar{\tau}_n \geq \bar{\tau}_a + \bar{\tau}_b$. Since a large range in the delay $\bar{\tau}_n$ is of interest, only this dark gray region will be considered in the next section. It is noted that this is not restrictive since typical values of $\bar{\gamma}$ and $\bar{\eta}$ are of $\mathcal{O}(0.1)$.

The axial dynamics is directly influenced by the torsional dynamics via the delay $\bar{\tau}_n$, which varies continuously as a function of the rotational speed. Therefore, to analyze the effect of the delay on the axial limit cycle, Fig. 6 is considered. It is clear that the delay has a major influence on the axial limit cycle. First, the length of the stick phase is driven by the delay, which influences the period time of the axial limit cycle. Here, the length of the slip phase is hardly affected. Since the average value of the scaled relative velocity z_2 equals zero, an increase in the length of the stick phase leads to an increase in the amplitude of the oscillation in the slip phase. This also increases the average value of z_1 for

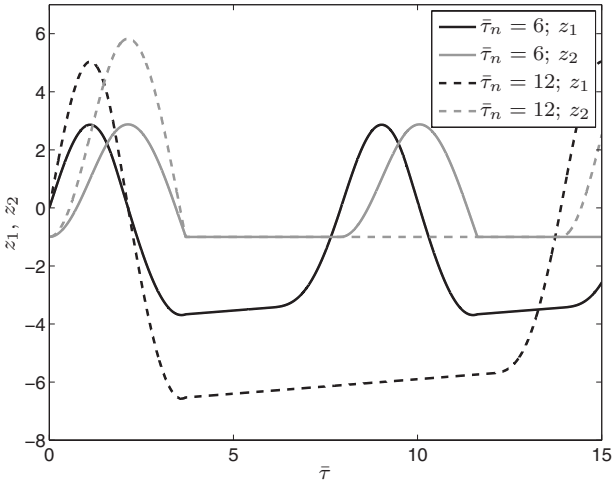

Fig. 6 Influence of the delay $\bar{\tau}_n$ on the axial limit cycle for $\bar{\gamma}$ =0.1 and $\bar{\eta}^2$=0.1

increasing delay.

For the stick-slip limit cycle, it has to be noted that the average wearflat forces are smaller than the nominal wearflat forces. The nominal wearflat force is based on a constant positive downward velocity, such that the full wearflat force is mobilized continuously. The stick-slip limit cycle causes the wearflat force to decrease in the stick phase, yielding lower forces on average. Since the average rate of penetration has to equal the imposed axial velocity at the surface, the decrease in average wearflat force is compensated by an elongation of the drill string. When the axial stiffness is not taken into account and a constant hook load is applied at the surface, as in Ref. [23], the response differs. Namely, a decrease in the average contact forces on the drill bit, caused by the axial vibrations, leads to a higher rate of penetration. Finally, since the decrease in the average wearflat forces is dependent on the delay (and the rotational speed), this effect is of importance in the analysis of the torsional dynamics. Thereto, the axial dynamics will be averaged in the next section.

3.6 Averaged Axial Response. In Sec. 4, it will be shown that the averaged wearflat force, characterized by the nonlinearity $\hat{g}$, is of importance in the torsional dynamics. By averaging Eq. (18), the average value $\langle \hat{g} \rangle_a$ of the nonlinearity can be expressed as a function of z_1 as follows:

$$\langle \hat{g} \rangle_a = -\frac{\bar{v}_0}{\lambda} \langle z_1 \rangle_a \tag{41}$$

where it is noted that the averaged value of the scaled acceleration $\langle z_2' \rangle_a$ equals zero. In the slip phase, z_1 represents the scaled acceleration of the bit. Since the slip phase connects two stick phases, where the velocity $dU/dt=0$ ($z_2=-1$), the average value of z_1 over the slip phase equals zero. Hence, the average value $\langle z_1 \rangle_a$ of z_1 over one limit cycle can be calculated by evaluating the stick phase only, leading to

$$\langle z_1 \rangle_a = \frac{1}{T}\left\{ \int_0^{\bar{\tau}_n - \bar{T}_{\text{slip}}} z_1^c(s)ds + \int_0^{\bar{\tau}_a} z_1^d(s)ds + \int_0^{\bar{\tau}_b - \bar{\tau}_a} z_1^e(s)ds \right\} \tag{42}$$

The averaged value $\langle z_1 \rangle_a$ is dependent on the system parameters $\bar{\gamma}$ and $\bar{\eta}^2$ and the delay $\bar{\tau}_n$ only.

As an example, the limit cycle with $\bar{\gamma}$=0.1 and $\bar{\eta}^2$=0.1 is analyzed for a wide range of the delay $\bar{\tau}_n$. The results are depicted in Fig. 7, which shows the averaged value $\langle z_1 \rangle_a$ and the minimum value $z_{1,\min}$ of $z_1(\bar{\tau})$ in the stick phase, which both appear to be linear with the delay. To show this, a linear fit $\langle z_1 \rangle_a^{\text{fit}}$ is depicted as

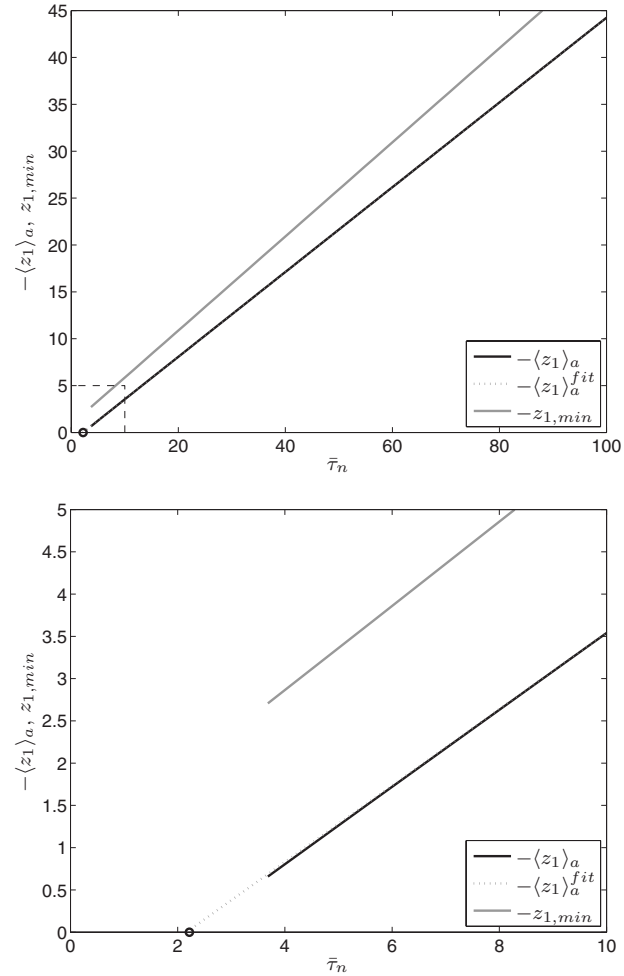

Fig. 7 Averaged value $\langle z_1 \rangle_a$ and minimum value $z_{1,\min}$ for the axial limit cycle with $\bar{\gamma}$=0.1 and $\bar{\eta}^2$=0.1. The black circle denotes the critical delay, at which stability is lost. The bottom graph is a zoomed version of the top figure.

well, which is extrapolated for small $\bar{\tau}_n$. Here, it has to be noted that no results are available for small $\bar{\tau}_n$ since the calculation of the axial limit cycle only holds when $\bar{\tau}_n \geq \bar{\tau}_a + \bar{\tau}_b$. Next, the critical delay $\bar{\tau}_n^{\text{crit}}$ at which stability of the equilibrium point is lost is shown as a circle. This critical delay is a result of the stability analysis in Sec. 3.1. The zoomed graph (bottom) in Fig. 7 shows that the extrapolated linear fit intersects the critical delay, such that the averaged value $\langle \hat{g} \rangle_a$ of the nonlinearity can be written as

$$\langle \hat{g} \rangle_a = -\frac{\bar{v}_0}{\lambda} \langle z_1 \rangle_a \approx \frac{\bar{v}_0}{\lambda} A(\bar{\gamma}, \bar{\eta})(\bar{\tau}_n - \bar{\tau}_n^{\text{crit}}(\bar{\gamma}, \bar{\eta})) \tag{43}$$

Here, $A(\bar{\gamma}, \bar{\eta}) > 0$ is the slope of $\langle z_1 \rangle_a$, which is dependent on the parameters $\bar{\gamma}$ and $\bar{\eta}$. Next, it has to be noted that $\bar{\tau}_n > \bar{\tau}_n^{\text{crit}}$, such that the axial equilibrium point is unstable. Further, $\bar{v}_0$ and λ are both positive, yielding a positive average value $\langle \hat{g} \rangle_a$. Since $g=0$ corresponds to the full contact force and $g=1$ models the absence of contact, this corresponds to a decrease in the average wearflat force for increasing delay, as is concluded before.

The magnitude of the minimum value of $z_1(\bar{\tau})$ increases with the delay but cannot grow unbounded. Namely, since $z_{1,\min}$ is related to the maximum value of the nonlinearity, the following condition holds:

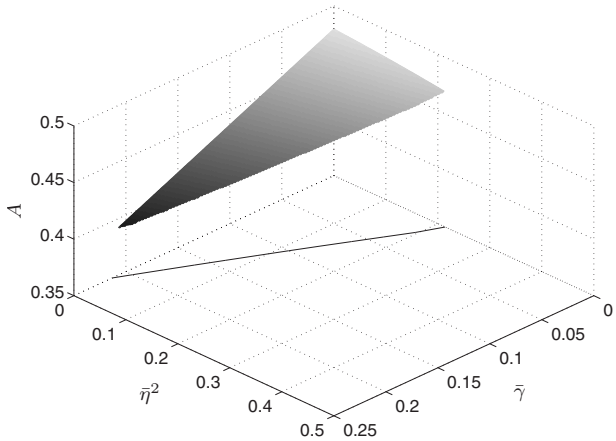

Fig. 8 Value of A in $(\bar{\gamma}, \bar{\eta}^2)$-space

$$-z_{1,\min} = \frac{\lambda}{\bar{v}_0} g_{\max} \leq \frac{\lambda}{\bar{v}_0} \tag{44}$$

When the condition in Eq. (44) does not hold, the wearflat force cannot compensate all the other forces at $dU/dt=0$ and the bit does not stick. Instead, it will move upward. Even though this does not necessarily cause bit bouncing (depth-of-cut $d<0$), it is a good indication for its occurrence in practice. This implies that bit bouncing is less likely to occur for bits with large wearflats (large λ), at a low rate of penetration $\bar{v}_0$ or small delay $\bar{\tau}_n$, which corresponds to high rotational speed ω_0. Here, it has to be noted that the delay plays a role via its influence on $z_{1,\min}$, as can be seen in Fig. 7.

The value of $A(\bar{\gamma}, \bar{\eta})$ as a function of the parameters $\bar{\gamma}$ and $\bar{\eta}$ is depicted in Fig. 8. To calculate $A(\bar{\gamma}, \bar{\eta})$, the averaged value $\langle z_1 \rangle_a$ is calculated for a range in the delay $\bar{\tau}_n$, similar to Fig. 7. Since a range in the delay $\bar{\tau}_n$ is needed, this is only done in the region where the calculation of the limit cycle holds for all $\bar{\tau}_n \geq \bar{\tau}_a + \bar{\tau}_b$, which is the dark gray region in Fig. 5.

As can be seen in Fig. 8, the value of $A(\bar{\gamma}, \bar{\eta})$ mainly depends on the damping $\bar{\gamma}$; the dependence on the stiffness $\bar{\eta}^2$ is minor.

In this section, the fast axial dynamics are analyzed. Since the axial equilibrium point, corresponding to constant downward motion, is unstable, small perturbations lead to an axial stick-slip limit cycle. An exact characterization of this limit cycle is given using a semi-analytical approach. Here, parts of the axial limit cycle are calculated analytically, whereas numerical optimization is used to determine the unknown parameters. An analysis of the limit cycle shows that the average wearflat forces decrease for increasing delay (i.e., for decreasing rotational velocity), which corresponds to the results of the model without axial stiffness and damping as in Ref. [23].

4 Torsional Dynamics

In the previous section, the axial dynamics is analyzed under the assumption that the parameters related to the slow torsional dynamics are constant. For the analysis of the torsional dynamics, the parameters related to the fast axial dynamics can be approximated by their averaged values. More specifically, these parameters are approximated by the averaged value over one axial limit cycle for the current (slowly varying) delay. Thus, exploiting the averaging of the axial dynamics in Eq. (9) yields

$$\ddot{\varphi}(\tau) + \varphi(\tau) = -n v_0(\tau_n(\tau) - \tau_{n0}) + n\beta\lambda\langle \hat{g} \rangle_a \tag{45}$$

Here, it has to be noted that the averaged value of the nonlinearity over one limit cycle is equal in all coordinate systems.

For this averaging approximation of the axial dynamics to be valid, the axial limit cycle has to exist. This holds in the region where the axial equilibrium point is unstable and no bit bouncing occurs. Next, the analytical calculation of the limit cycle can be used when the conditions $\bar{\tau}_a \leq \bar{\tau}_b$ and $\bar{\tau}_a + \bar{\tau}_b \leq \bar{\tau}_n$ hold, as shown in Sec. 3.5.

During a typical torsional limit cycle, the delay varies and might even be small enough to stabilize the axial dynamics, which can occur at high rotational speed. On the other hand, the bit can stick torsionally. During torsional stick, the bit also sticks axially since it is assumed that the rock cannot be indented. The approximation in Eq. (45) is invalid in these cases and is therefore only valid in a part of the torsional dynamics. Nonetheless, the approximation can be used close to the torsional equilibrium point, which corresponds to a constant rotational speed of the bit $d\Phi/dt>0$. Next, the condition that the axial equilibrium point is unstable has to hold, i.e., $\bar{\tau}_{n0} > \bar{\tau}_n^{\text{crit}}$, with $\bar{\tau}_{n0} = 2\pi/(n\omega_0)$. Then, substituting Eq. (43) in Eq. (45) gives

$$\ddot{\varphi}(\tau) + \varphi(\tau) = -n v_0(\tau_n(\tau) - \tau_{n0}) + n\beta\bar{v}_0 A(\bar{\gamma}, \bar{\eta})(\bar{\tau}_n(\tau) - \bar{\tau}_n^{\text{crit}}(\bar{\gamma}, \bar{\eta})) \tag{46}$$

Here, the first term at the right-hand side $(-n v_0(\tau_n - \tau_{n0}))$ corresponds to the averaged cutting forces, whereas the second term $(n\beta\bar{v}_0 A(\bar{\tau}_n - \bar{\tau}_n^{\text{crit}}))$ represents the averaged wearflat forces. Next, A and $\bar{\tau}_n^{\text{crit}}$ are constant for a set of parameters $\bar{\gamma}, \bar{\eta}$, while the delay varies with time. It is recalled that the delay τ_n is defined by the implicit Eq. (10). However, it is beneficial for the analysis of the torsional dynamics to have an explicit expression for the delay. Thereto, a first-order Taylor approximation of the delayed relative angular position $\varphi(\tau - \tau_n)$ is used:

$$\varphi(\tau - \tau_n) \approx \varphi(\tau) - \dot{\varphi}(\tau)\tau_n \tag{47}$$

The delay τ_n is typically of $\mathcal{O}(0.1)$, while the characteristic time of the torsional vibrations is 2π, which justifies the approximation. When combining Eq. (47) with Eq. (10), the delay can be written as

$$\tau_n(\dot{\varphi}(\tau)) \approx \frac{2\pi}{n(\omega_0 + \dot{\varphi}(\tau))} \tag{48}$$

Substituting this in Eq. (46) yields an autonomous nonlinear approximate of the torsional dynamics. This approximate is linearized around $\dot{\varphi}=0$ $(d\Phi/dt>0)$ to determine local stability properties, yielding

$$\ddot{\varphi}(\tau) + \varphi(\tau) = n v_0 \beta A(\tau_{n0} - \tau_n^{\text{crit}}) - n v_0(\beta A - 1)\frac{2\pi}{n\omega_0^2}\dot{\varphi}(\tau) \tag{49}$$

Here, the relation $\bar{v}_0\bar{\tau}_n = v_0\tau_n$ is used. In practice, bits are commonly characterized by $\beta<1$. Next, Fig. 8 shows that $A<1$ for realistic parameter values $\bar{\gamma}, \bar{\eta}$. Therefore, the term $\beta A - 1$ will in general be negative, and the torsional equilibrium point is thus unstable. Instability of the torsional equilibrium leads to torsional limit cycling and, possibly, torsional stick-slip. On the other hand, a high β can stabilize the torsional dynamics, where it is recalled that $\beta = \zeta\mu\xi$ is dependent on the geometry of the drill bit. Since β characterizes the influence of the wearflat forces on the torsional dynamics, a high influence of these forces will stabilize the torsional dynamics, indicating that the wearflat forces do not generate the velocity-weakening effect. This can also be concluded from Eq. (46), where it is recalled that an increase in the torsional velocity decreases the delay. An increasing rotational speed decreases the length of the stick phase, such that the averaged wearflat force increases, causing an apparent damping. On the other hand, the cutting forces are velocity weakening, as can be concluded from Eq. (46) as well. For increasing rotational speed, the averaged depth-of-cut decreases because of the constant downward velocity, leading to lower cutting forces. For small β, the influence of the cutting forces is larger than the wearflat forces, yielding a net velocity-weakening effect in the torsional dynamics.

Hence, the fast axial vibrations form the onset of the torsional vibrations. This conclusion is similar to that for the drilling system as analyzed in Ref. [23], where the effects of axial stiffness and damping were not included. Thus, even though the addition of axial stiffness and damping does significantly change the axial limit cycles, the main qualitative effects on the torsional dynamics remain unchanged for realistic parameter values.

5 Conclusions

In this work, the drill string model introduced in Ref. [16] and analyzed in Ref. [23] is extended with the essential aspects of axial stiffness representing the axial flexibility of the drill string and viscous friction representing dissipation along the bottom hole assembly. Both aspects are relevant in practice such that the model extensions lead to a more realistic model. In the original work in Ref. [16], the weight-on-bit is assumed to be constant and compression or elongation of the drill string is not taken into account. Since this is unrealistic for a vibrating drill bit, the axial flexibility is included in the model in this paper, where a constant rate of penetration is imposed at the surface.

For the original model in Ref. [16], the mechanisms leading to torsional stick-slip oscillations are analyzed in Ref. [23]. In the current work, it is analyzed whether these mechanisms are still valid for the extended and more realistic model.

As in Ref. [23], the axial dynamics are analyzed individually, which is rooted in the separation of time scales between the fast axial and slow torsional dynamics. For realistic parameter values, the axial equilibrium point is unstable, and the drill bit experiences axial stick-slip oscillations, where the stick phase is caused by the discontinuity in the contact forces. In Ref. [23], an approximation of the axial limit cycle is obtained analytically. Due to the additional model complexity caused by the axial damping and stiffness, this approach is not possible for the extended model in the current work. Instead, a semi-analytical approach to calculate the exact limit cycle is developed.

The analysis approach exploits the fact that an analytic expression of the axial limit cycle can be found, where numerical optimization is used to find the unknown parameters. This approach allows for an efficient and accurate analysis of the axial stick-slip limit cycle. Here, it is noted that the applicability of this semi-analytical approach is not limited to the analysis of drilling systems. For example, it is foreseen that this analysis can be applied to mechanical systems with Coulomb friction.

The axial stick-slip limit cycle is dependent on the rotational speed of the drill bit and therefore has an effect on the torsional dynamics, which is analyzed by averaging the axial dynamics. Here, two opposing effects play a role. First, the average cutting forces generate an apparent velocity-weakening effect in the torsional dynamics. Second, the average wearflat forces generate an apparent velocity-strengthening effect. For realistic bit parameters, the overall effect is velocity weakening, explaining the onset of torsional vibrations that might lead to torsional stick-slip. This result further validates the conclusions of Ref. [23] for a more realistic model, indicating that, as long as the axial stiffness and damping parameters are not excessively large, the mechanisms responsible for the onset of torsional vibrations are qualitatively unchanged.

The analysis of the onset of torsional vibrations might lead to new active control strategies for drilling systems. Namely, the onset of torsional stick-slip vibrations is driven by the axial dynamics, such that stabilization of these axial dynamics may also prevent torsional vibrations. Similar observations were made in Refs. [10,25]. However, the analysis methodology proposed in this paper can facilitate the design and performance evaluation of novel controllers for the axial dynamics. Moreover, existing control strategies targeting the torsional dynamics directly [11,26,27] should be tested on the current model as well.

Acknowledgment

Part of this work is done in cooperation with Emmanuel Detournay and Thomas Richard of the Drilling Mechanics Group, CSIRO Petroleum in Perth, Australia. They are gratefully acknowledged for their contribution.

References

[1] Challamel, N., 2000, "Rock Destruction Effect on the Stability of a Drilling Structure," J. Sound Vib., **233**(2), pp. 235–254.
[2] Christoforou, A. P., and Yigit, A. S., 2003, "Fully Coupled Vibrations of Actively Controlled Drillstrings," J. Sound Vib., **267**(5), pp. 1029–1045.
[3] Jansen, J. D., 1993, "Nonlinear Dynamics of Oilwell Drillstrings," Ph.D. thesis, Delft University of Technology, Delft, The Netherlands.
[4] Khulief, Y. A., Al-Sulaiman, F. A., and Bashmal, S., 2007, "Vibration Analysis of Drillstrings With Self-Excited Stick-Slip Oscillations," J. Sound Vib., **299**(3), pp. 540–558.
[5] Tucker, R. W., and Wang, C., 1999, "An Integrated Model for Drill-String Dynamics," J. Sound Vib., **224**(1), pp. 123–165.
[6] van den Steen, L., 1997, "Suppressing Stick-Slip-Induced Drillstring Oscillations: A Hyperstability Approach," Ph.D. thesis, University of Twente, The Netherlands.
[7] Brett, J. F., 1992, "The Genesis of Torsional Drillstring Vibrations," SPE Drilling Engineering, **7**(3), pp. 168–174.
[8] Leine, R. L., van Campen, D. H., and Keultjes, W. J. G., 2002, "Stick-Slip Whirl Interaction in Drillstring Dynamics," ASME J. Vibr. Acoust., **124**(2), pp. 209–220.
[9] Mihajlović, N., van Veggel, A. A., van de Wouw, N., and Nijmeijer, H., 2004, "Analysis of Friction-Induced Limit Cycling in an Experimental Drill-String System," ASME J. Dyn. Syst., Meas., Control, **126**(4), pp. 709–720.
[10] Yigit, A. S., and Christoforou, A. P., 2006, "Stick-Slip and Bit-Bounce Interaction in Oil-Well Drillstrings," ASME J. Energy Resour. Technol., **128**(4), pp. 268–274.
[11] Jansen, J. D., and van den Steen, L., 1995, "Active Damping of Self-Excited Torsional Vibrations in Oil Well Drillstrings," J. Sound Vib., **179**(4), pp. 647–668.
[12] Pavone, D. R., and Desplans, J. P., 1994, "Application of High Sampling Rate Downhole Measurements for Analysis and Cure of Stick-Slip in Drilling," Proceedings of the SPE 69th Annual Technical Conference and Exhibition, Paper No. SPE 28324, pp. 335–345.
[13] Nishimatsu, Y., 1972, "The Mechanics of Rock Cutting," Int. J. Rock Mech. Min. Sci., **9**, pp. 261–270.
[14] Detournay, E., and Defourny, P., 1992, "A Phenomenological Model for the Drilling Action of Drag Bits," Int. J. Rock Mech. Min. Sci. Geomech. Abstr., **29**, pp. 13–23.
[15] Detournay, E., Richard, T., and Shepherd, M., 2008, "Drilling Response of Drag Bits: Theory and Experiment," Int. J. Rock Mech. Min. Sci., **45**(8), pp. 1347–1360.
[16] Richard, T., 2001, "Self-Excited Stick-Slip Oscillations of Drag Bits," Ph.D. thesis, University of Minnesota, MN.
[17] Richard, T., Germay, C., and Detournay, E., 2007, "A Simplified Model to Explore the Root Cause of Stick-Slip Vibrations in Drilling Systems With Drag Bits," J. Sound Vib., **305**, pp. 432–456.
[18] Dareing, D., Tlusty, J., and Zamudio, C., 1990, "Self-Excited Vibrations Induced by Drag Bits," ASME J. Energy Resour. Technol., **112**(1), pp. 54–61.
[19] Elsayed, M. A., Dareing, D. W., and Dupuy, C. A., 1997, "Effect of Downhole Assembly and Polycrystalline Diamond Compact (PDC) Bit Geometry on Stability of Drillstrings," ASME J. Energy Resour. Technol., **119**(3), pp. 159–163.
[20] Tucker, R. W., and Wang, C., 2003, "Torsional Vibration Control and Cosserat Dynamics of a Drill-Rig Assembly," Meccanica, **38**(1), pp. 145–161.
[21] Baumgart, A., 2000, "Stick-Slip and Bit-Bounce of Deep-Hole Drillstrings," ASME J. Energy Resour. Technol., **122**(2), pp. 78–82.
[22] Germay, C., Denoël, V., and Detournay, E., 2009, "Multiple Mode Analysis of the Self-Excited Vibrations of Rotary Drilling Systems," J. Sound Vib., **325**(1–2), pp. 362–381.
[23] Germay, C., van de Wouw, N., Nijmeijer, H., and Sepulchre, R., 2009, "Nonlinear Drillstring Dynamics Analysis," SIAM J. Appl. Dyn. Syst., **8**(2), pp. 527–553.
[24] Lagarias, J. C., Reeds, J. A., Wright, M. H., and Wright, P. E., 1998, "Convergence Properties of the Nelder-Mead Simplex Method in Low Dimensions," SIAM J. Optim., **9**(1), pp. 112–147.
[25] Elsayed, M. A., and Raymond, D. W., 2002, "Analysis of Coupling Between Axial and Torsional Vibration in a Compliant Model of a Drillstring Equipped With a PDC Bit," Proceedings of the ASME Engineering Technology Conference on Energy, pp. 897–904.
[26] de Bruin, J. C. A., Doris, A., van de Wouw, N., Heemels, W. P. M. H., and Nijmeijer, H., 2009, "Control of Mechanical Motion Systems With Non-Collocation of Actuation and Friction: A Popov Criterion Approach for Input-to-State Stability and Set-Valued Nonlinearities," Automatica, **45**(2), pp. 405–415.
[27] Navarro-López, E. M., 2009, "An Alternative Characterization of Bit-Sticking Phenomena in a Multi-Degree-of-Freedom Controlled Drillstring," Nonlinear Anal.: Real World Appl., **10**(5), pp. 3162–3174.